JACS
JOURNAL OF THE AMERICAN CHEMICAL SOCIETY
Article
Cite This: J. Am. Chem. Soc. 2019, 141, 3444−3455
pubs.acs.org/JACS

Genesis and Stability of Hydronium Ions in Zeolite Channels

Meng Wang,[†] Nicholas R. Jaegers,[†,‡] Mal-Soon Lee,[†] Chuan Wan,[†] Jian Zhi Hu,*[,†] Hui Shi,[†] Donghai Mei,[†] Sarah D. Burton,[†] Donald M. Camaioni,[†] Oliver Y. Gutiérrez,[†] Vassiliki-Alexandra Glezakou,[†] Roger Rousseau,[†] Yong Wang,[†,‡] and Johannes A. Lercher*[,†,§]

[†]Institute for Integrated Catalysis, Pacific Northwest National Laboratory, Richland, Washington 99354, United States
[‡]Voiland School of Chemical Engineering and Bioengineering, Washington State University, Pullman, Washington 99163, United States
[§]Department of Chemistry and Catalysis Research Center, TU München, Lichtenbergstrasse 4, 85748 Garching, Germany

Supporting Information

ABSTRACT: The catalytic sites of acidic zeolite are profoundly altered by the presence of water changing the nature of the Brønsted acid site. High-resolution solid-state NMR spectroscopy shows water interacting with zeolite Brønsted acid sites, converting them to hydrated hydronium ions over a wide range of temperature and thermodynamic activity of water. A signal at 9 ppm was observed at loadings of 2−9 water molecules per Brønsted acid site and is assigned to hydrated hydronium ions on the basis of the evolution of the signal with increasing water content, chemical shift calculations, and the direct comparison with $HClO_4$ in water. The intensity of $^{1}H-^{29}Si$ cross-polarization signal first increased and then decreased with increasing water chemical potential. This indicates that hydrogen bonds between water molecules and the tetrahedrally coordinated aluminum in the zeolite lattice weaken with the formation of hydronium ion−water clusters and increase the mobility of protons. DFT-based *ab initio* molecular dynamics studies at multiple temperatures and water concentrations agree well with this interpretation. Above 140 °C, however, fast proton exchange between bridging hydroxyl groups and water occurs even in the presence of only one water molecule per acid site.

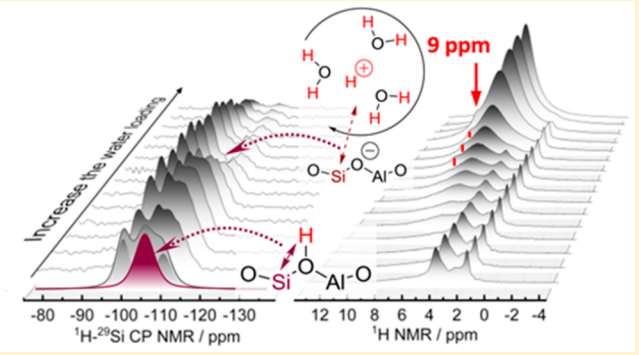

INTRODUCTION

Acidic zeolites are widely used for dehydration, cracking, dehydrogenation, isomerization, and alkylation.[1−4] All of these reactions are catalyzed by protons originating from bridging hydroxyl groups that balance anionic sites generated upon incorporation of trivalent cations into the zeolite framework.[5−8] These proton-donor groups exhibit moderate to high acid strength and readily donate protons to substrate or solvent molecules (e.g., alkenes, aromatic molecules, alcohols, and water).[9−12]

The thermodynamic state of Brønsted acid sites (BAS) and its interactions with molecules in the fluid phase have been extensively studied by a variety of physicochemical techniques as well as theoretical calculations.[1,11−13] The mechanisms of reactions catalyzed by BAS have been established by kinetic studies and spectroscopic observations of key intermediate species.[5−8,10] Understanding the impact of (co)reactants and solvents on elementary steps of catalytic cycles involving BAS is, however, in its very early stages. In particular, characterizing the role of water on the nature and action of BAS is of key importance, because it is the solvent of choice for the conversion of polar substrates and it is frequently generated as co-product.[14−18]

At low pressures, water negatively influences dehydration of alcohols by stabilizing, for example, adsorbed 1-propanol significantly more than the transition state to dehydration.[18] For alkane C−H bond activation, reaction rates increased by a factor of 10 in the presence of low amounts of water (≤1 water molecule per BAS), but high water loadings (>2 or 3 water molecules per BAS) decreased rates.[15] Reactions in condensed phase are also significantly impacted by the nature of the proton-donor site. The mechanism of cyclohexanol dehydration changes as the nature of the proton-donating site switches from bridging OH groups to hydrated hydronium ions.[10] Olefin protonation by a hydronium ion has a significantly higher barrier than protonation by a bridging hydroxyl group.[19] On the other hand, the formation and size of the hydronium ion in the zeolite pores limit the adsorption of substrates, decreasing reaction rates, although the intrinsic reactivity of the hydronium ions remains invariant.[20] Thus, characterization of water interacting with acid sites and substrates in confined environments is critical for a molecular description of reaction mechanisms. It is also a step toward a quantitative under-

Received: July 27, 2018
Published: January 30, 2019

DOI: 10.1021/jacs.8b07969
J. Am. Chem. Soc. 2019, 141, 3444−3455

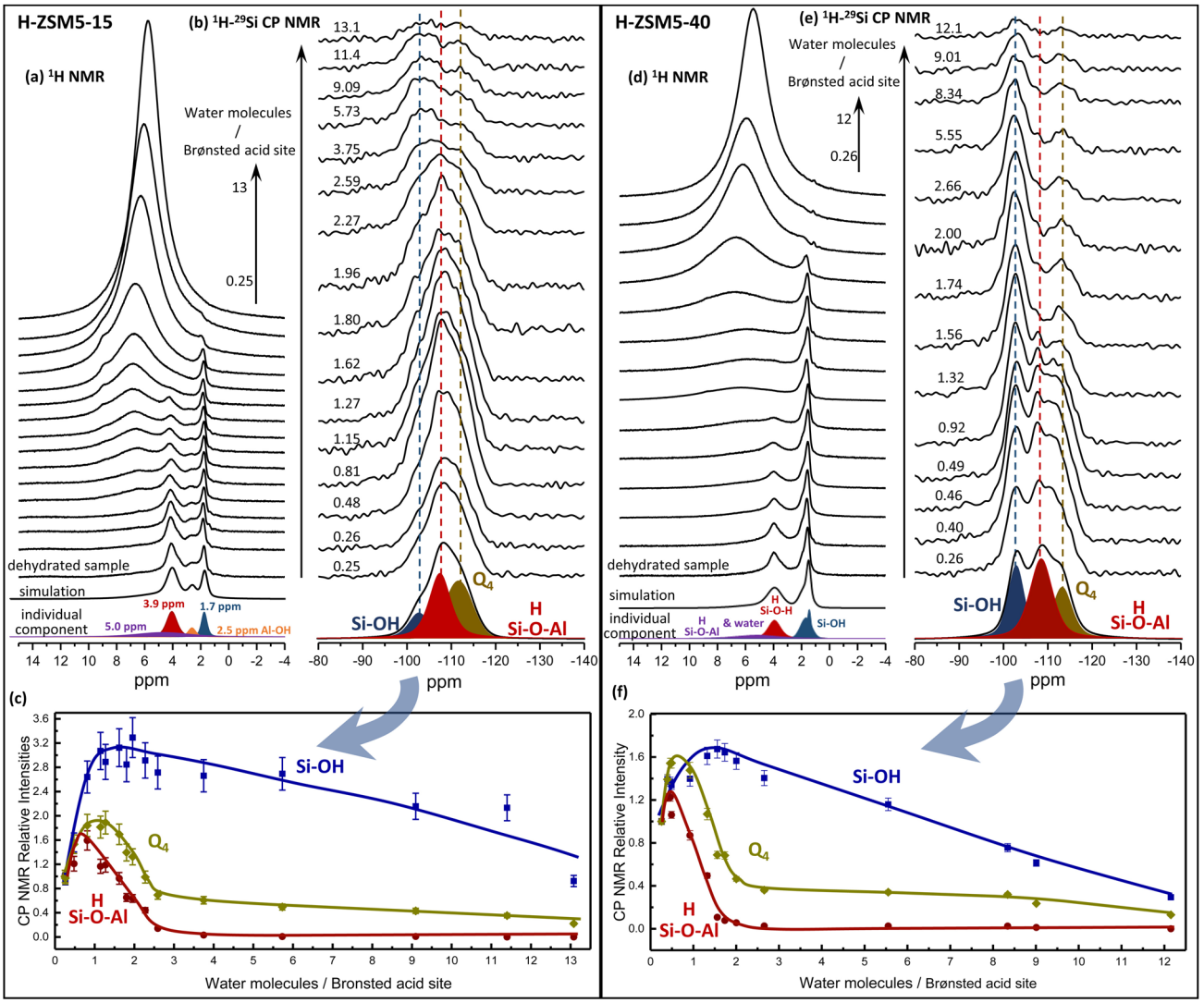

Figure 1. ^{1}H one-pulse and $^{1}H-^{29}Si$ cross-polarization (CP) MAS solid-state NMR spectra and dependencies of CP signal relative intensities of zeolites on water loading of dehydrated zeolites. (a, b) Parallel comparison of ^{1}H and CP ^{29}Si MAS spectra of dehydrated H-ZSM5-15 zeolite hydrated with indicated amounts of water (water molecules per Brønsted acid site were calculated from spin-counting); from bottom to top, the water molecules increased from 0.25 to 13. ^{1}H spectra were measured before and after the $^{1}H-^{29}Si$ CP spectrum; the changes of water molecules during the experiments were less than 5%. The cross-polarization contact time was 3 ms, spinning speed was 5 kHz, recycle delay was 5 s, and the number of scans was 20 000. All spectra in each set are shown with real heights. Here, the CP MAS experiments for all the samples were conducted using the same instrument parameters to semiquantitatively detect the interaction between ^{1}H and ^{29}Si. The deconvolution of the first ^{1}H NMR and CP ^{29}Si spectrum is shown at the bottom of a and b, different species are color coded, and the intensities of these species are normalized to 1, with the increasing of water molecules; the dependencies of these relative intensities from the CP ^{29}Si spectrum are shown in c. (d, e, and f) Representative NMR spectra and CP signal intensities of H-ZSM5-40 zeolite. Q_4 represents $[(Si(OSi)_4]$ species.

standing of empirical concepts put forward to explain the interactions of zeolites with water.[21]

Studies addressing the properties of the Brønsted acid sites and the zeolite framework in the presence of water in the channels[22−42] have shown that a number of species coexist (i.e., BAS, Lewis acid sites with strongly bound water, water hydrogen-bonded to BAS, hydronium ion clusters, physically adsorbed water), depending on the thermodynamic activity of water.[43,44] Yet, identification of the conditions under which these different species exist has not been quantitative, because of the lack of experimental access to information about the state of the adsorbed water under reaction conditions.

In the present study, we combine, therefore, systematic NMR and IR spectroscopic studies with density functional theory (DFT)-based and ab initio molecular dynamics calculations to discern both the chemical environment and the mobility of protons over a wide range of pressure and temperature. We will show how this approach has enabled identifying the nature of hydrated hydronium ions under conditions typically used for catalysis.

RESULTS AND DISCUSSION

Identification of Brønsted Acid Sites: From Framework Hydroxyl to Hydrated Hydronium Ions. Initially, the fully dehydrated H-ZSM5-15 and H-ZSM5-40 and samples that were exposed to 0.005 mbar of water for increasing periods of time were analyzed by IR spectroscopy. Spectra (Figure S1) show the band for bridging hydroxyls at 3609 cm^{-1} to gradually decrease under N_2 flow (room temperature). This suggests that less than one water per BAS was initially

DOI: 10.1021/jacs.8b07969
J. Am. Chem. Soc. 2019, 141, 3444−3455

Table 1. Concentrations of Different Proton Species of the Freshly Dehydrated HZSM-5 Zeolites

						^{1}H NMR spin counting,[f] [μmol/g]				
						Si-OH	Al-OH	Si-OH-Al	Si-(OH···OH_2)-Al[h]	
H-ZSM5	Si/Al[a]	Al_{ICP},[b] [μmol/g]	Al_{NMR},[c] [μmol/g]	Al_F/Al_{EF},[d] [μmol/g]	BAS/LAS,[e] [μmol/g]	1.7 ppm	2.5 ppm	3.9 ppm	5.0 ppm	H_2O/BAS[g]
15	15.9	995 (5.7)	1040 (6.0)	894/101 (5.1/0.6)	784/156 (4.5/0.9)	370 ± 10	182 ± 5	717 ± 20	625 ± 20	0.25 ± 0.05
40	40.8	398 (2.3)	408 (2.4)	394/4 (2.3/0.02)	367/46 (2.1/0.3)	550 ± 20		410 ± 20	190 ± 20	0.26 ± 0.05

[a]Si/Al determined from ICP-OES. [b]Concentration of Al determined by ICP. [c]Determined from ^{27}Al MAS NMR spectra of the fully hydrated zeolite (Figure S3); spin-counting relative to an external standard.[49] [d]The total concentration of aluminum was calculated from ICP; the percentages of tetrahedrally coordinated framework Al (Al_F) (the theoretical maximum quantity of BAS) and octahedrally coordinated extra-framework Al (Al_{EF}) were determined from ^{27}Al MAS NMR. [e]Quantification of BAS (Brønsted acid sites) and LAS (Lewis acid sites) using pyridine adsorption. [b−e]Number of Al or H sites per unit cell are shown in parentheses. [f]The amounts of different H species were obtained from ^{1}H NMR spectral deconvolutions (Figure 1a and d). [g]The H_2O/BAS ratio is calculated as $0.5 \times [H_{\delta=3.9} + H_{\delta=5.0} - Al_F]/Al_F$. [h]Si-(OH···$OH_2$)-Al indicates H-bonded BAS and strongly adsorbed water.

present, because this band is known to disappear after the stoichiometry reaches one water molecule per BAS on H-ZSM5.[26] Two bands at 2400 and 2900 cm^{-1} appeared when the sample was exposed to flowing N_2 with 5 ppm water and gradually increased over time, while the band for the bridging hydroxyl groups disappeared.[25,27] These two bands are attributed to hydrogen-bonded water on BAS, reaching the maximum intensity at H_2O/BAS equal to 1.[25,26] At even longer exposures (e.g., 12 h), more water molecules were adsorbed and the 2400 and 2900 cm^{-1} bands decreased, being gradually replaced by a broad band at 3600−2800 cm^{-1}.

Seeking quantitative information on the genesis of different H species, we turned to NMR spectroscopy to characterize samples with selected numbers of water interacting with BAS. Figure 1a and d show ^{1}H one-pulse solid-state magic angle spinning (MAS) NMR spectra of dehydrated (see Experimental Methods) samples of H-ZSM5-15 and H-ZSM5-40 with different amounts of water adsorbed (0.25 to 13 H_2O/BAS). For the freshly dehydrated samples (the bottom spectra of Figure 1a and d), three main peaks appeared, i.e., narrow ones at 1.7 ppm (with small shoulders slightly downfield) and 3.9 ppm and a broad one at 5 ppm. There is also a small 2.5 ppm peak from HZSM5-15 (Figure 1a). The signals at 1.7 and 2.5 ppm are assigned to silanol groups (Si-OH) and hydroxyl groups associated with external framework Al (Al-OH), respectively.[45−47] The relatively sharp peak at 3.9 ppm is attributed to unperturbed Brønsted sites, whereas the broad peak at 5 ppm represents Brønsted sites that are hydrogen bonded to another framework oxygen or to water.[45,46] Its presence in the activated zeolite suggests that water from trace moisture (about 5 ppm) in the N_2 gas used during pretreatment and NMR measurements has been adsorbed on the zeolite. This conclusion is supported by the broad H-bonded feature at about 5 ppm (Figure 1a and d), which grew larger over a span of 2 weeks (Figure S2).

Table 1 shows the concentration of the different proton species in the freshly dehydrated HZSM-5 zeolites. The data are derived from ^{1}H NMR spin-counting, bulk Al concentrations from inductively coupled plasma and framework Al concentrations from quantitative analysis of the ^{27}Al MAS NMR spectra (Figure S3).[48] The concentrations of the unperturbed BAS (3.9 ppm) in H-ZSM5-15 and H-ZSM5-40 were 0.7 and 0.4 mmol/g, respectively. Including the broad resonances at 5 ppm that correspond to both H-bonded BAS and adsorbed water, the average molar ratio between water and BAS (H_2O/BAS) was calculated to be 0.25 and 0.26 for H-ZSM5-15 and H-ZSM5-40, respectively.

Under N_2 (Figure S2) the maximum concentration of water molecules adsorbed were 2.5 and 2.7 per BAS for H-ZSM5-15 and H-ZSM5-40, respectively, according to spin-counting NMR results. In contrast, water loadings of up to 12 or 13 water molecules per BAS were obtained by equilibrating the sample packed in the NMR rotor in a desiccator over a saturated $Ca(NO_3)_2$ aqueous solution. Thus, a series of ^{1}H NMR spectra were obtained for zeolite samples of different hydration levels, i.e., 0.25−13 water molecules per BAS (Figure 1a and d for the two zeolites).

Interaction between Water and SiOHAl Sites during Hydration. ^{1}H−^{29}Si cross-polarization (CP) NMR is used to monitor the evolution of the acid site structure during the hydration process. Important differences are noted between the single-pulse ^{29}Si NMR spectra with the CP spectra for the dehydrated and fully hydrated samples (Figure S4). For the single-pulse experiments, the highest peaks appeared at −110 to −120 ppm, which are attributed to [$(Si(OSi)_4$] sites as the dominating species in relatively high Si/Al ratio zeolites; these peaks were partially lost in the CP experiments.[50−52] Two peaks, −102 ppm and −106 to −108 ppm, at terminal Si−OH ([$Si(OSi)_3OH$]) or SiOHAl ([$Si(OSi)_3OHAl$]) regions were detected in the CP experiments. The ^{29}Si resonance is expected to have a greater downfield shift upon interaction with a proton, leading to a lesser extent of shielding relative to trivalent Al ions replacing a nearby Si atom.[52] Therefore, the peak at −102 ppm is assigned to [$Si(OSi)_3OH$] (the Si bonded to a terminal silanol OH group), and the peak at −106 to −108 ppm to [$Si(OSi)_3OHAl$] (Si in a T site bonded to one framework Al atom). The concentration of framework Al (Al_F) is comparable to that of SiOH groups, like in H-ZSM5-40 (Table 1, SiOHAl = 394 μmol/g and SiOH = 550 μmol/g). Indeed, these peaks were similar in intensity in the dehydrated sample (bottom spectrum in Figure 1e). The signal for SiOHAl ([$Si(OSi)_3OHAl$]) decreased in the hydrated sample (upper spectra in Figure 1e) because the bridging hydroxyl group donates the proton to water when more water is adsorbed.

The contributions of the three Si species, [$(Si(OSi)_4$], SiOHAl ([$Si(OSi)_3OHAl$]), Si−OH ([$Si(OSi)_3OH$]), are deconvoluted in the ^{1}H−^{29}Si CP NMR spectrum of the sample with the lowest water concentration (bottom in Figure 1b and e). The evolution of the intensities of these signals as a

DOI: 10.1021/jacs.8b07969
J. Am. Chem. Soc. 2019, 141, 3444−3455

function of water loading was similar for the two zeolites (Figure 1c and f). With the concentration of water approaching one molecule per BAS, the intensities of all signals increased due to the proximity of additional protons at fixed (and close) positions at framework sites. This is illustrated by the dashed arrow in Figure 2a that depicts a

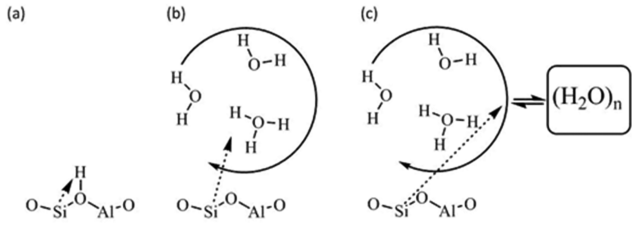

Figure 2. Representation of BAS environment for (a) bare acid site, (b) low water concentrations with hydronium ion formation, and (c) high water concentrations with extended phase. Dotted arrows suggest relative H−Si distances, whereas solid arrows indicate chemical exchange between protons.

H^+ relatively close to the Si, where a single water molecule would simply add nearby protons to polarize the Si atom, while not dramatically increasing the H−Si distance or enhancing the proton mobility. These $^1H-^{29}Si$ CP NMR results prove that the distance between the ^{29}Si and the ^1H in the T site remains relatively small and invariant up to 1 water molecule per BAS.

The CP signal from SiOHAl ($[Si(OSi)_3OHAl]$) then decreased with increasing water loading, almost disappearing at two water molecules per BAS. This suggests a decrease in the dipolar interaction due to the elongation of the distance between the ^1H and ^{29}Si nuclei forming H_3O^+ and an enhanced mobility in the presence of two water molecules. This is depicted by the dashed line in Figure 2b showing both an increased H−Si distance (dotted arrow) and enhanced mobility (solid arrow). The CP signal associated with $[(Si(OSi)_4]$ entities changed with water loading in a similar way to SiOHAl ($[Si(OSi)_3OHAl]$), probably because the main signal of the $[(Si(OSi)_4]$ was obtained from the ^1H on the bridging hydroxyl through the cross-polarization.

At three water molecules, the signal from SiOHAl ($[Si(OSi)_3OHAl]$) completely disappeared. When more water molecules were adsorbed, the signal of the SiOHAl ($[Si(OSi)_3OHAl]$) remained negligible and the signal from silanol groups gradually dropped due to enhanced proton mobility, as illustrated by Figure 2c, showing molecular exchange with water not directly associated with the hydronium ion cluster.

DFT calculations show that the distance between the framework oxygen and hydrogen is 0.977 Å in the absence of adsorbed water molecules. This distance increases to 1.041 Å when one water molecule is adsorbed on the framework Al. The difference of about 0.064 Å is small compared to the variations observed with larger water cluster sizes, i.e., 0.977 → 1.041 → 1.426 Å as the cluster increases from 0 to 2 (Figure 3 and Table 3).

Interaction between Water and Hydroxyls during Hydration. The signal at 4 ppm in the ^1H NMR spectra (10th spectrum, Figure 1a, left panel) was visible at H_2O/BAS ratios of up to approximately 2. The appearance of a different species, the generation of a hydronium ion, leads to the complete disappearance of the proton signal of the SiOHAl group (11th spectrum, Figure 1, left panel). The relative intensities of the

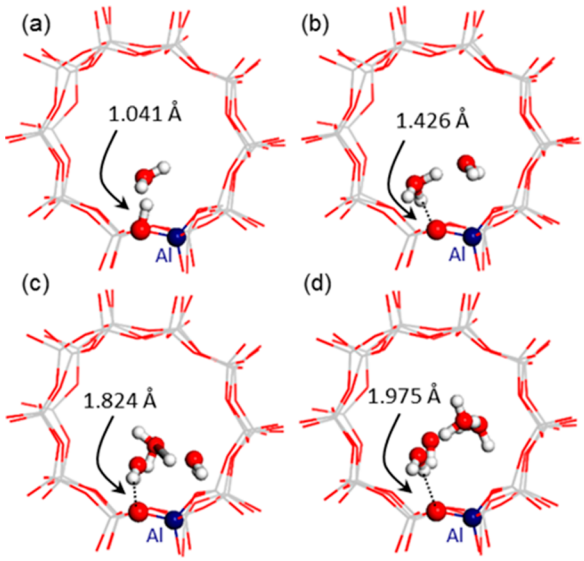

Figure 3. Structures illustrating the hydrating process in the H-ZSM5 zeolite channel with increasing numbers of water molecules optimized by DFT cluster calculations. From a to d, the number of water molecules increases from 1 to 4 with the shortest O−H distance labeled in each instance.

Table 2. Spin−Spin Relaxation Time of Different H Species in the H-ZSM5 Zeolites

species	chemical shift, ppm	T_2, ms[a]	H_2O/BAS[b]
SiOH groups	1.7	10[c]	<10
BAS	4	3[d]	<2
water and H-bonded BAS	5−8	<0.5[e]	>0
hydronium ion	9	∼1[f]	1.6−9.1[g]
			1.3−5.5[g]

[a]Spin−spin relaxation time (T_2) was determined by spin−echo experiments with different pulse distance for H-ZSM5-15 and H-ZSM5-40 under similar water loadings. [b]The range of water molecules per Brønsted acid site when the relevant species was observed. [c]T_2 for silanol was measured with 0.25, 1.3, and 2.0 H_2O/BAS. [d]T_2 for Brønsted acid was measured with 0.25 H_2O/BAS. [e]T_2 for water and H-bonded BAS acid was measured with 0.25 and 1.3 H_2O/BAS. [f]T_2 for hydronium ion was measured with 1.6 and 2.0 H_2O/BAS. [g]The 9 ppm signal was observed in the range of 1.6−9.1 and 1.3−5.5, for H-ZSM5-15 and H-ZSM5-40, respectively.

silanol-related signal (1.7 ppm) and bridging hydroxyl-related signal (4 ppm) in ^1H NMR experiments are plotted in Figure S5 as a function of the H_2O/BAS ratio. The ^1H NMR signal for the bridging hydroxyl group and the CP signal from the corresponding Si disappeared at ∼2 water molecules per BAS. When loading exceeded 3 water molecules per BAS, the ^1H NMR signal of silanol decreased as did the related $^1H-^{29}Si$ CP signal (shown in Figure 1c and f).

Having established the location and mobility of the protons, let us next examine these proton species during the hydration process. Each ^1H NMR peak exhibited significantly different line widths. Increasing MAS rates beyond 5−6 kHz did not further narrow the line widths because the hydrogen spins are diluted.[53] Differences in line widths likely arise from the distribution of chemical shifts and different spin−spin relaxation times (T_2) ($\nu_{1/2} = 1/\pi T_2$).[33,54,55] The distribution of chemical shifts is attributed to a distribution of local environments that could include varying water mobility. By

DOI: 10.1021/jacs.8b07969
J. Am. Chem. Soc. 2019, 141, 3444−3455

Table 3. ^{1}H NMR Chemical Shift for Different Proton Species during H-ZSM5 Zeolite Hydration from DFT Calculation[a]

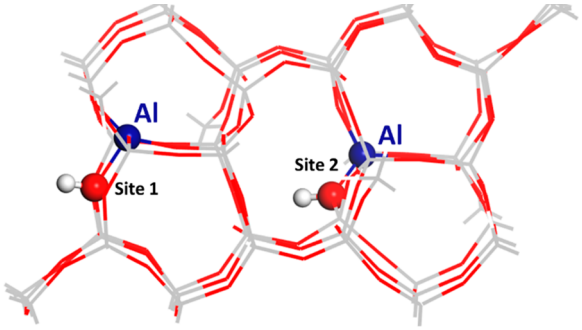

H_2O/BAS	site 1		site 2	
	R_{O-H}, Å[b]	average chemical shift, ppm[c]	R_{O-H}, Å	average chemical shift, ppm[c]
0	0.977	3.7	0.982	4.5
1	1.041	6.9	1.049	7.5
2	1.426	10.2	1.139	8.5
3	1.824	7.5	1.452	8.8
4	1.975	8.1	1.773	8.8

[a]Geometry-optimized structures for H-ZSM15 with two different sites. The other structures are shown in Figure S12. [b]Distance between the proton from the bridging hydroxyl group and the oxygen. [c]The average chemical shift of all the protons.

using different pulse widths in spin−echo experiments (Figure 4a−j), T_2 was measured (Table 2) for the hydrogens in different chemical environments, and the signals could be selectively suppressed to isolate individual peaks and provide more detail on their chemical environment.[33,55]

The dehydrated zeolites (Figure 4a for H-ZSM5-15 and Figure 4f for H-ZSM5-40) showed two distinguishable signals, SiOH and SiOHAl groups, with T_2 being 10 and 3 ms, respectively. A third peak, visible in Figure 4a at 2.8 ppm corresponding to extra-framework Al-OH groups, is not relevant for the discussion here. With adsorption of 2 H_2O/BAS, the broad peak at 5−8 ppm dominated the spectra with the shortest T_2 (<0.5 ms), which is assigned to a combination of adsorbed water and hydrogen-bonded BAS sites. When a small echo delay time of, for example, 1 ms, was used to suppress the broad signal, a small narrow peak at 9 ppm was observed at H_2O/BAS ratios of 1.6−9.1 for H-ZSM5-15 (1.3−5.5 for H-ZSM5-40). This species showed a longer T_2 (~1 ms) than adsorbed water (5−8 ppm). The shaded area in Figure 4 highlights the range of H_2O/BAS ratios where the 9 ppm peak can be distinguished. At H_2O/BAS ratios higher than 9, this 9 ppm feature was masked by a strong broad peak (Figure 4e and j).

The structure of the BAS as a function of adsorbed water was explored by ab initio molecular dynamics (AIMD) simulations. The calculations showed that the structures of systems with water/BAS ratios of 1, 2, 8, and 16 in H-ZSM-5 at 27 °C (Figure S6, upper panel) are similar to the static DFT results (Figure 3). In Figure 5, we show the calculated radial

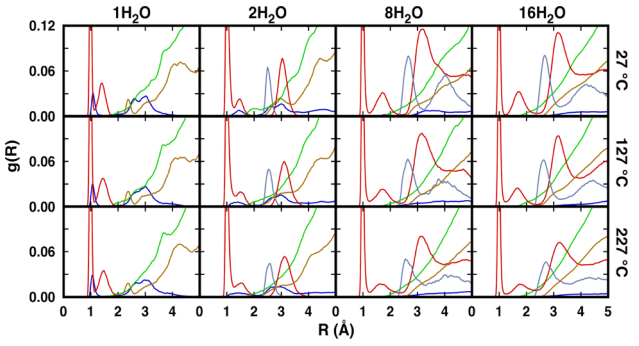

Figure 5. Radial distribution function $g(R)$ at different temperatures with water/BAS ratios of 1:1, 2:1, 8:1, and 16:1 obtained from AIMD simulations. Line color codes of $g(R)$: red for O_W-H, blue for O_B-H, green for O_Z-H, gray for O_W-O_W, and gold for H-Si.

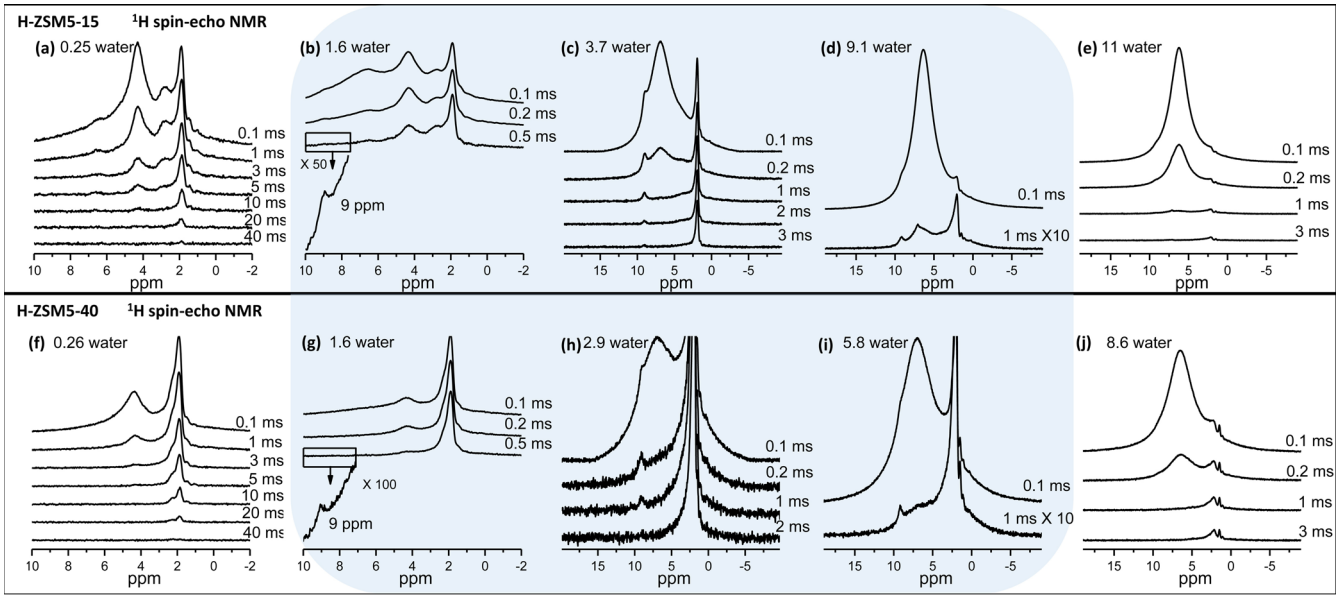

Figure 4. (a−j) Comparison of ^{1}H spin−echo MAS NMR spectra of different water loading on the zeolites acquired with varying echo times. Spinning rate was 9.5 kHz, and the echo time varied from 0.1 to 40 ms. The recycle delay was 10 s, and 16−1024 scans were acquired depending on the signal/noise. The shaded areas indicate the range of H_2O/BAS ratios when the signal at 9 ppm appeared.

DOI: 10.1021/jacs.8b07969
J. Am. Chem. Soc. 2019, 141, 3444−3455

distribution function (RDF), which gives average distances between different species, i.e., oxygen of water to all H (Ow-H), oxygen in BAS to all H (O_B-H), oxygen in the framework (except O_B) to all H (Oz-H), oxygens in water molecules (O_W-O_W), and Si-H.

The RDF of O_B-H (blue line in Figure 5) shows an increased bond length with water/BAS ratio increasing from 0 to 2 (0.98 Å with 0 H_2O, 1.08 Å with 1 H_2O, and 1.45 Å with 2 H_2O). Consistent with static DFT calculations, showing proton dissociation at >2 water molecules (see Figure 3), MD trajectories with 8 and 16 water molecules show that the distance of O_B−H is >3 Å, indicating complete dissociation of the proton from the BAS (Figure 5). The dissociation of the proton is further confirmed by the RDF of H−Si (gold line in Figure 5), which shows the disappearance of a peak around 2.3 Å with increasing water content. We note that the structure of the local coordination environment about the H_3O^+ is identical for 8 and 16 H_2O systems (Figure 5), indicating the formation of a stable $H_3O^+(H_2O)_7$ cluster. These results agree well with the CP signals from SiOHAl in the NMR (see Figure 1). However, for all cases RDF of O_Z-H (green line in Figure 5) shows a very small broad peak around 2 Å due to weak interaction between framework oxygens and the hydrogen atoms.

The hydration of the proton is indicated by the RDF of O_w-H. Small peaks in the O_w-H RDF at 1.4−1.8 Å in Figure 5 represent hydrogen bond formation between a hydroxyl group and water or between water and H_3O^+.[55] For the system with a water/BAS ratio of 1, water forms a hydrogen bond with a hydroxyl group, showing a peak at 1.4 Å. With 2 water/BAS, the acid proton is transferred to a water molecule, forming H_3O^+ (green circle in Figure S6b), where it interacts with OB and the other O_w via a hydrogen bond (peaks at ∼1.45 Å for blue and red lines in Figure 5, respectively). This change corresponds to the disappearance of the SiOHAl signal with 2 water/BAS ratio, as shown in Figure 1. However, proton diffusion between two water molecules is not observed at 27 °C within our simulation time period (100 ps). With 16 water molecules per BAS, the peak at ∼1.8 Å in RDF of O_w-H, along with the peak at ∼4.3 Å in the RDF of O_w-O_w, indicates water cluster formation via hydrogen bonds. By visualizing structural dynamics, we observed that there are two groups of water: one forming a cluster with 7 or 8 water molecules including H_3O^+, the other either forming a cluster with a size of ∼4 or being free water. At 27 °C, proton hopping occurs only among the nearest neighbor water molecules for a short time, as illustrated in Figure 2b. The proton hopping will be discussed in a later section.

The stoichiometries for water interacting with SiOH groups are consistent with water adsorption and infiltration isotherms at room temperature.[56−58] At water loadings below 4 H_2O/BAS, water is located exclusively at SiOHAl ($[Si(OSi)_3OHAl]$) groups.[58] With increasing partial pressure, water begins to interact with Si-OH ($[Si(OSi)_3OH]$) and with hydrated hydronium ions.[56−59] Under near-saturation conditions, the adsorption capacity in the micropore of the zeolite is limited by the concentration of SiOHAl ($[Si(OSi)_3OHAl]$) and Si-OH ($[Si(OSi)_3OH]$),[56,57] while additional water adsorption occurs at the external crystal surface and mesopores.[56,60,61] For our experiments at water loadings of approximately 10 H_2O/BAS, water molecules associate with both the SiOHAl ($[Si(OSi)_3OHAl]$) and Si-OH ($[Si(OSi)_3OH]$) in the micropore as well as on the external surface, but these sites are indistinguishable in the NMR spectra.

Characterization of the Hydronium Ion in Zeolite Confines. The narrow peak at about 9 ppm has been observed before on, for example, hydrated H-Y zeolite with Si/Al = 2.6 and attributed to $Al(H_2O)_6^{3+}$ formed via hydration of extra-framework Al.[29−33] We note, however, that the concentrations of extra-framework Al in these two H-ZSM5 zeolites (Table 1) are significantly lower than those studied previously, especially H-ZSM5-40, which drastically reduces the likelihood of $Al(H_2O)_6^{3+}$ observation by ^{1}H NMR. In the case of H-ZSM5-15 containing 10% of external framework Al the Al-OH species was unchanged, despite the 9 ppm peak growing in with increasing the concentration of water (Figure S7). Moreover, the signal of $Al(H_2O)_6^{3+}$ in HY zeolite was observed to continuously shift downfield from 7 ppm and continuously narrow (until it reaches 9.1 ppm) with nominally increasing to 26 water molecules per unit cell.[29] In contrast, the chemical shift and half line-width of the peak at 9 ppm in this study did not change with increasing concentrations of adsorbed water (Figure 4a−j) over the range 0.25 < H_2O/BAS < 13. Moreover, a solid-state NMR characterization of $Al(H_2O)_6(NO_3)_3{\cdot}3H_2O$ in combination with theoretical models ($Al(H_2O)_6^{3+}{\cdot}nH_2O$ with n = 0 and 12) shows that the peak at 9 ppm cannot in this case be attributed to $Al(H_2O)_6^{3+}$ (see additional discussion, Figures S8 and S9, and Table S1−S3 in the Supporting Information). A free hydronium ion in aqueous phase is expected to have a chemical shift in the range of 7−12 ppm.[31,33] However, we show in the SI (see additional discussion and Figures S10 and S11) that, in the confines of H-ZSM-5, the chemical shift is effectively 9 ppm. This was established by observing the peak to increase when small amounts of concentrated $HClO_4$ solutions were added to the zeolite. This assignment of the H_3O^+ at 9 ppm in the zeolite was also corroborated by theoretical simulations.

We used theoretical calculations of the ^{1}H NMR chemical shift of the proton species by adding a specified number of water molecules into H-ZSM5 zeolite cluster models. The representation consisted of two different T sites with 0−4 water molecules per BAS (Table 3). The results show that with one water molecule adsorbed, the bridging O−H bond length is slightly elongated to give a chemical shift of approximately 7 ppm. However, the proton is completely transferred to a cluster of three water molecules (Figure 3 and Table 3). With two or more water molecules, the average chemical shifts of all protons in the cluster are approximately 9 ppm (9.4 ppm for two, 8.2 ppm for three, and 8.5 ppm for four water molecules), assuming fast exchange between the acid proton and protons from water in these clusters (Figure 2b). The inclusion of more than 4 H_2O/BAS (Table S4) shows that with exchange among the water molecules the chemical shifts are lowered to 7.0, 6.6, 6.3, 6.6, and 6.2 ppm for 5, 6, 7, 8, and 9 water molecules, respectively.

Average chemical shifts like those listed in Table 3 are expected when there is a quick exchange among all H species. For instance, Hunger et al. reported that the fast proton exchange among the water molecules in the hydronium ion cluster gives rise to a signal observable at 5−8 ppm in zeolite H-Y.[33] In contrast, we can differentiate several H species in ZSM5 with water loadings below 2 H_2O/BAS, probably because water molecules are heterogeneously distributed among all acid sites. Enhanced exchange with an extended

DOI: 10.1021/jacs.8b07969
J. Am. Chem. Soc. 2019, 141, 3444−3455

water phase (as illustrated by the solid arrows in Figure 2c) would decrease the observed chemical shift (Table S4).

Impact of Temperature. The spectra in Figure 6 (right side) show that in situ experiments follow the observations

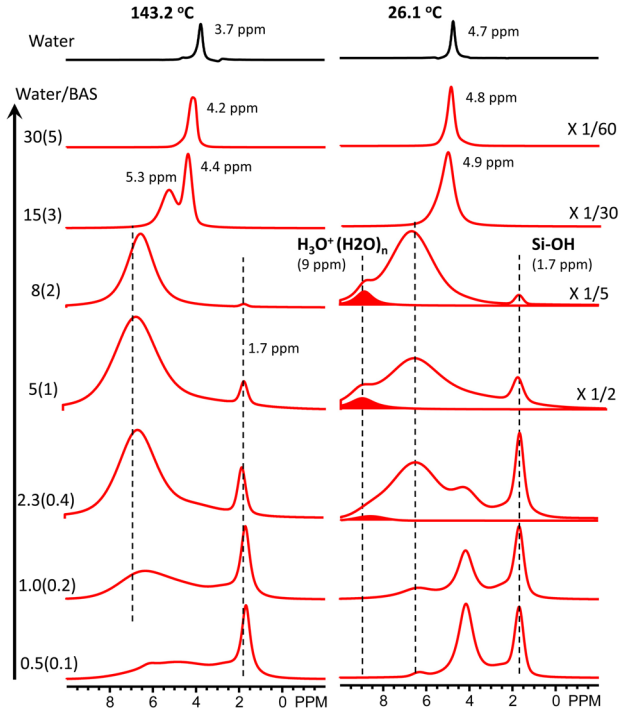

Figure 6. Comparison of ^{1}H one-pulse NMR spectra of H-ZSM5-15 loaded with different amounts of water at different temperatures. The spinning rates were from 3400 to 3760 Hz and ±10 Hz in each experiment. The rotor was heated to 143 °C and measured first, then cooled to room temperature. All thermal effects were reversible. The numbers of water, calculated from spin counting, are listed on the left of each spectrum. In parentheses are the uncertainties, which are due mainly to imperfect background subtraction and spinning sidebands.

described above for ex situ studies (Figures 1 and 4). Narrow peaks corresponding to silanol groups and Brønsted acid sites were observed for samples with low water content. The intensity of the acid site signal (4 ppm) decreased monotonically with the increasing water loading, while the peak area of water and hydrogen-bonded hydroxyl groups (6.5 ppm) increased. The 9 ppm signal was also observed with similar water loading (2.3−8 H_2O/acid site) to the ex situ experiments (Figure 1). With more than 15 water molecules per BAS, all signals merged together and could not be differentiated at room temperature.

Spectra recorded at 143 °C (left panel of Figure 6) displayed peaks of silanol groups (1.7 ppm) at the same chemical shift and with the same widths at half-height as those observed at room temperature, suggesting a limited effect of temperature on the mobility of this stable (nonacidic) OH group. The peaks related to the BAS (4−8 ppm) were significantly broadened compared to their room-temperature counterparts. Even with less than one water molecule per BAS, the Brønsted acid site was almost invisible and the 9 ppm peak never appeared across the broad range of water loadings investigated. We hypothesize that the signals for hydronium ion, water, and the Brønsted acid site merged due to fast proton exchange among these species at the elevated temperature. Indeed, molecular dynamics studies indicate that water clusters that are relatively stable at room temperature and low loading become highly disordered and mobile at elevated temperatures.[62] This mobility induces exchange between species over a range of chemical environments. In line with this high mobility, the center of the broad peak shifted downfield, when the water loading increased from 0.5 to 5 at 143 °C, indicating more weight to species related to, for example, the 9 ppm peak.

At 0.5 and 1.0 H_2O/BAS ratios (Figure S13a and b), the sidebands from Brønsted acid signals were relatively stronger than the sidebands from the terminal silanol groups at room temperature. This is attributed to the dipolar interaction between the hydrogen in the bridging hydroxyl group and the neighboring aluminum.[63] The sidebands from the BAS were significantly suppressed at temperatures higher than 83 °C, where the signal at 4 ppm was also absent due to broadening that decreased both the intensities of the peak and its sidebands. The line width of the single broad peak at about 6.2 ppm became narrower with increasing temperature, and no change was observed in the silanol peak and its sidebands. Thus, we conclude that the quick proton exchange among water molecules and acid sites in the framework increases with temperature even with water loadings below 1 H_2O/BAS. With 2.3 H_2O/BAS, the broad peak observed between 4 and 8 ppm (Figure S13c), which narrowed without a change in chemical shift, indicates that quick proton exchange occurs at temperatures above 53 °C.

When 15 water molecules were added, the signal at about 4.9 ppm at room temperature divided into two peaks at 143 °C (Figure S13d). These resonance changes/peak divisions indicate the presence of different types of water (adsorbed in the zeolite channel and outside of the pore) which do not quickly exchange between each other at this temperature and water loading. The upfield signal (lower ppm) behaved like the resonance from pure water (the dashed lines in the inset of Figure S13d), shifting upfield without any change in the line width. The chemical shift of the low-field signal (5.3 ppm) remained constant, while slightly narrowing with increasing temperature, consistent with the behavior of the broad peak (5−8 ppm; Figure S13c) at lower water loadings. Therefore, free water (outside the micropores) and water strongly associated with the hydronium ion are distinguished at this water loading.

With nominally 30 water molecules per acid site, all zeolite proton species were involved in quick exchange. As we have determined that a hydrated water cluster has approximately eight water molecules, the other water molecules are best characterized as free water outside of the zeolite channel.[64] It should be noted in passing that all observed changes with temperature were fully reversible.

To address these different species, we performed AIMD simulations to determine how temperature affects the structure of differently sized water clusters in H-ZSM-5 pores. The calculated RDFs for 1, 2, 8, and 16 water molecules per BAS at 27, 127, and 227 °C are shown in Figure 5. The results show that with 2 water molecules at the BAS at 27 °C, the proton is transferred to a water molecule. For the 8 and 16 H_2O systems there are strong reductions in the intensities at ~1.8 Å for O_w-H and at ~4.3 Å for O_w-O_w, indicating substantial restructuring of the water network. As discussed above, the 16 H_2O system shows two kinds of water, one forming a cluster with H_3O^+ in the size of 7 or 8 H_2O and the other becoming free water in the high-temperature regime. This result agrees with the two peaks observed with 15 water/BAS at 143 °C in ^{1}H NMR

DOI: 10.1021/jacs.8b07969
J. Am. Chem. Soc. 2019, 141, 3444−3455

spectra (see Figure 6). In Figure S14, we show a histogram of distance difference $\Delta R = R_1 - R_2$ as a function of time where R_1 represents the H_a-O_B distances and R_2 the shortest distance between H_a and O_w with H_a being the nearest neighbor of O_B, where negative values indicate H_a near the BAS and positive values indicate H_a closer to water. In addition, $\Delta R \approx 0$ indicates Zundel-like structure ($H_5O_2^+$), while $\Delta R < 0$ indicates the formation of eigen-like structure ($H_3O^+(H_2O)_3$).[65−67] With 1 H_2O, the proton is at the BAS at all simulated temperatures. With 2 water/BAS, the Zundel-like structure is formed and stable. Interestingly two distinguishable peaks are formed as temperature increases, indicating that the system fluctuates between two states: the proton at the BAS and the hydronium ion. This is consistent with the peak at ∼7 ppm in the ^{1}H one-pulse NMR spectrum observed with 2.3 water/BAS at 143 °C (see Figure 6). With 16 H_2O the proton has moved away from the BAS, forming a hydronium ion that is completely hydrated at all temperatures.

To quantify the water confinement effect, we compare oxygen distributions in the system of 8 H_2O in HZSM-5 and protonated 8 H_2O in the gas phase. For this, we define the probability of $R-R_{COM}$, $P(R-R_{COM})$, which measures the distance between the center of mass (COM) and oxygen atoms (see Figure 7). In addition, we plot the partial

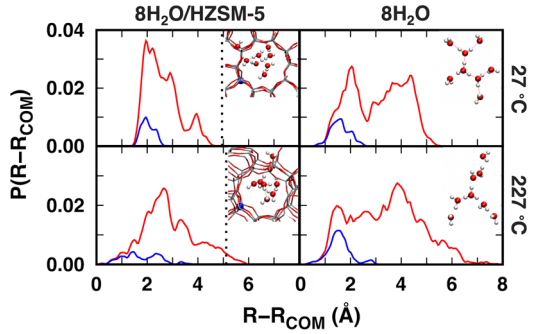

Figure 7. Probability of distance between O and COM with 8 H_2O in HZSM-5 (left column) and the gas phase (right column) at 27 and 227 °C. Red line is for all oxygen atoms, and blue is for oxygen of H_3O^+ only.

probability of H_3O^+ (blue line in Figure 7) as well as the average distance of the BAS site from the COM (dotted line in the left column of Figure 7). In general, the confined cluster in the zeolite is more compressed than in the gas phase. In the confined cluster 90/75% of the density is within 4 Å from COM at 27/227 °C. In contrast, in the gas phase cluster at 27 °C the cluster forms two shells around the central H_3O^+, having 3 and 4 waters in the first and second shell, respectively. At 227 °C, however, the distribution broadens out such that over 50% of the density is greater than 4 Å away from the COM. Conversely, the H_3O^+ in the zeolite resides in the core of the cluster at 27 °C and becomes much more mobile at 227 °C as opposed to more localized in the gas phase. Overall, the confinement compresses the water cluster and enhances the proton mobility in the system. We thus conclude that the confined water cluster is chemically distinct from its gas-phase analogue.

To understand dynamic properties of the H_3O^+, we calculated its population decay correlation function $C(t)$ in the 16-water system using

$$C(t) = \frac{\langle h(0)\, h(t)\rangle}{\langle h\rangle}$$

where $h = 1$ if O_w of interest forms H_3O^+ and $h = 0$ otherwise.[68] $C(t)$ at different temperatures is shown in Figure S15, and as expected proton transfer takes place in shorter time with increased temperature. We note that $C(t) \sim \exp(-Dt)$ where D is the proton hopping rate and estimated from the linear fit to $-\ln C(t)$; see the inset of Figure S15. Obtained D values enabled us to estimate the proton-hopping activation energy (E_a) by fitting to the Arrhenius equation (Figure 8).

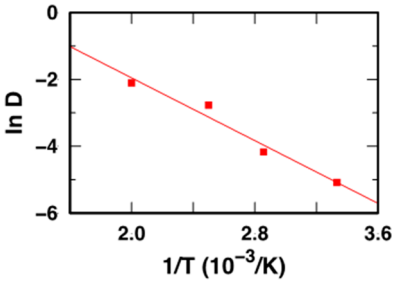

Figure 8. Arrhenius plot of proton hopping rate whose slope gives proton-hopping activation energy.

The $E_a \approx 18$ kJ/mol is somewhat larger than values reported for bulk water (E_a = 8.4−13 kJ/mol).[69] This indicates that proton mobility is hindered in the presence of confined water.

CONCLUSIONS

We directly monitored the interaction between hydrogen species and silicon at the T site by ^{1}H−^{29}Si CP MAS NMR. Quantitative spectral analysis showed the boundary conditions for the genesis, evolution, and stability of hydronium ions in HZSM5 pores.

Bridging hydroxyl groups are stable at water loadings of one H_2O/BAS or below. At these conditions, the O−H bond is elongated due to hydrogen bonding with the water molecule, but the proton remains bound to the Al T-site in the framework. The hydronium ion is formed upon proton transfer when two water molecules interact with the bridging hydroxyl group. We have unambiguously correlated this event with the appearance of a signal at 9 ppm in the ^{1}H NMR spectra. The hydronium ion has a longer spin−spin relaxation time than the strongly adsorbed water present at lower water loadings.

The 9 ppm signal is visible at room temperature from 1.6 to 9.1 waters per BAS for H-ZSM5-15 and 1.3 to 5.5 waters per BAS for H-ZSM5-40 and subsequently disappears at higher water loading as proton exchange becomes fast compared to the NMR time scale. In turn, this quick proton exchange among different hydrogen species leads to one peak resembling a bulk water signal.

At low water loadings of up to 7 or 8 H_2O/BAS, H_2O forms strong hydrogen bonds with H_3O^+, forming protonated water clusters. With higher loadings, interaction of the protonated clusters with additional water molecules is attenuated, approaching that for interaction with neutral water clusters and with Si-OH defects in the zeolite. Thus, at low water loadings, these Si-OH groups do not interact with water and so are visible in the ^{1}H NMR spectra. However, at loadings greater than ∼8 H_2O/BAS, the excess water interacts with these Si-OH groups, causing them to disappear due to fast exchange of water protons with the Si-OH proton. Based on

DOI: 10.1021/jacs.8b07969
J. Am. Chem. Soc. 2019, 141, 3444−3455

this trend (appearance−disappearance of unique hydrogens with H_2O loading), the fate of the extra-framework Al-OH is expected to be similar to that of the Brønsted acid site, but due to its very low abundance in the two samples studied, a detailed assessment is difficult here.

Calculations of oxygen distribution with respect to center of mass with 8 H_2O in HZSM-5 and gas phase from AIMD simulations show that the confined water is chemically different compared with that in gas phase, having more compressed structure but higher mobility. Based on theoretical estimates of proton hoping rates from AIMD simulations, a proton hopping activation energy is estimated to be 18 kJ/mol in a fully hydrated H-ZSM5, which is larger than that in bulk water. At elevated temperatures, the signals of all species related to the BAS (bridging hydroxyl group, hydrogen-bonded acid site, strongly adsorbed water, and hydronium ion) merged into one signal, even with less than one water per acid site.

Catalysis science has successfully exploited the shape selectivity of zeolites for catalytic reactions, precluding access or removal of reactants or products or hindering transition states by steric constraints. Beyond this effect, the stabilization of transition states allowed by such confines has been recently recognized as a key factor to enhance rates.[10,20] Here, even small changes in void size and shape may induce dramatic effects on the rate of demanding reactions. Whereas the size and acid strength of hydrated hydronium ions depends on the equilibration with water,[19] the size of the hydrated hydronium ions limits the possibility to take up organic reactants and their density controls the thermodynamic activity of organic reactants.[64] The findings of this work suggest that confined hydronium ions will have appreciably different catalytic activity than hydronium ions in bulk liquid phase. Thus, by advancing the understanding of the structure of hydronium ions in zeolites, this study markedly contributes to the understanding of the impact of water on reaction mechanisms in confined space.

EXPERIMENTAL METHODS

H-ZSM-5 Zeolite. The zeolites (Si/Al = 15 and 40) were obtained by calcination of the NH_4-form zeolites (CBV3024E and CBV8014 from Zeolyst International) at 450 °C under air flow and then stored for more than 2 days under ambient temperature and humidity prior to further treatment or measurements.

Infrared Spectroscopy. Infrared spectra were recorded on a ThermoScientific Nicolet FTIR spectrometer using an MCTA detector with a resolution of 2 cm^{-1}. Thirty-two scans were accumulated for each spectrum. Most experiments were measured at room temperature under a flow of house N_2. The acidity was probed by dosing pyridine onto the sample in a controlled way. The previously activated sample was allowed to equilibrate with pyridine vapors at 0.1 mbar for 1 h at 150 °C before removal of physisorbed pyridine at 10^{-4} mbar. By integration of the Brønsted and Lewis peaks (1565−1515 cm^{-1} and 1470−1430 cm^{-1}, respectively) and use of the molar extinction coefficients determined by Emeis[70] along with the disk weight, the concentrations of acid sites were quantified.

Solid-State NMR Spectroscopy. ^1H and ^{29}Si MAS solid-state NMR experiments were performed on a Varian-Agilent Inova wide-bore 300 MHz NMR spectrometer and confirmed with a Bruker 600 MHz NMR spectrometer at higher field, and ^{27}Al NMR were acquired from an 850 MHz spectrometer. Ex situ experiments were performed using commercial rotors of different diameters (2.5 and 5 mm). Detailed information about each measurement is presented in the figure captions. ^1H, ^{27}Al, and ^{29}Si spectra were referenced to tetramethylsilane (TMS at 0 ppm), 1.0 M $Al(NO_3)_3$ in water (0 ppm), and 4,4-dimethyl-4-silapentane-1-sulfonic acid (DSS at 1.534 ppm), respectively. The measurement uncertainty was ±0.1 ppm. After the rotor was loaded into the probe, spin counting techniques were used to estimate the H concentrations. The hydrogen concentrations were determined via integrating the spectral intensities ranging from 120 to −110 ppm and comparing to an external spin counting standard, adamantane. As all spectra were acquired at the same parameters and number of scans, they were normalized to the mass of each sample. The background NMR signals were measured using the same parameters on an empty rotor and subtracted from the spectra. In situ ^1H MAS NMR were carried out using a custom-made 7.5 mm high-temperature and high-pressure MAS rotor.[71,72]

$^1H-^{29}Si$ cross-polarization NMR was used to monitor the evolution of the acid site structure during the hydration process. The signal in the $^1H-^{29}Si$ CP MAS NMR spectrum is attributed to the transfer of magnetization from ^1H to ^{29}Si mediated by the dipolar interaction, meaning that the CP signals originate only from ^{29}Si in close proximity to ^1H nuclei. Thus, CP becomes more efficient as the distance between the ^{29}Si and the ^1H nuclei decreases or the adjacent ^1H nuclei increase in quantity or localization at a particular position. In the absence of ^1H nuclei near ^{29}Si atoms or in the case of increased mobility of ^1H increases, CP signals disappear.[30,73,74]

For the in situ ^1H NMR measurements of zeolite, the chemical shift values, spinning sidebands, and line widths observed in dehydrated zeolites have been used to infer the acid strength of bridging hydroxyl groups as well as the distance between hydroxyl protons and the framework aluminum.[75−80] Baba and co-workers showed that the chemical shift value was independent of the temperature, although the intensity of the spinning sidebands monotonically decreased, and the peak width increased from room temperature to about 100 °C before decreasing.[75,81]

Methods for Loading Water into the Zeolite Samples. Prior to ^1H MAS NMR experiments, the sample was put in a quartz tube, which was later connected to flowing nitrogen (10 mL/min) and heated to 400 °C for 10 h. The samples were then allowed to cool to room temperature and packed into NMR rotors in a dry nitrogen glovebox as soon as possible. Water was introduced to zeolite samples in vapor phase for the ex situ experiments (Figures 1 and 4, Tables 1 and 2) and liquid phase for the in situ tests (Figure 6). To adsorb water vapor, dehydrated zeolites were first sealed in the glovebox into NMR rotors and then transferred into the NMR probe by a sealed glass vial to avoid exposure to air during transit. After the relocation of the packed rotor, it was exposed to the nitrogen gas used to spin the NMR rotor. Even though a grooved Kel-F plunger/plug was used to seal the rotor, the sample still adsorbed the moisture from nitrogen slowly. The sample was considered equilibrated when the change of spectra was less than 1% over several days, after which the rotor was taken out while capped, but exposed to ambient humidity before returning to the probe for measurements. Alternatively, liquid water was injected into the unsealed rotor[71] using a microliter syringe, after which the rotor was sealed (Figure 6). The pressure in the sealed rotor varied from near ambient at room temperature to 1.4−5.3 bar (total pressure, water and balance N_2) at the elevated temperature of 143.2 °C, depending on the amount of water added to the rotor and the fraction adsorbed by the zeolite. Loadings were calculated gravimetrically, based on the concentration of framework Al site, and were verified with spin counting experiments leading to an error estimation of 10%. Since the homemade rotor is heavier and thicker than commercial rotors, an ethylene glycol temperature calibration was necessary for accurate temperature set points.

Structure Optimization and Chemical Shift Calculation. The Amsterdam Density Functional (ADF-2014) package[82] was applied to calculate the electronic structures. The generalized gradient approximation (GGA)-based Becke-Lee−Yang−Parr function with dispersion correction (BLYP-D)[83] was used for the geometry optimization. All calculations were performed at the Slater-type TZ2P basis set (triple-ζ, 2-polarization function, all-electron).[84] The geometry-optimized structures at the same level of theory were applied to calculate the chemical shielding for each atom with the same basis set. Tetramethylsilane was used as the ^1H chemical shift reference by converting the calculated shielding to the observed

DOI: 10.1021/jacs.8b07969
J. Am. Chem. Soc. 2019, 141, 3444−3455

shielding using the following equation: $\delta_{iso} = \sigma(TMS) - \sigma_{calc} = 31.4 - \sigma_{calc}$. H-ZSM5 clusters containing 58 T atoms were extracted from a previous periodic structure optimization,[85] cut to the size used in this study, and terminated with H atoms (Si−H bond lengths fixed at 1.455 Å) to replace terminal O atoms while maintaining peripheral charge neutrality, as established elsewhere.[86] Except for these charge-balancing protons, atoms exceeding two bonds from the Al site were frozen to maintain the integrity of the zeolite structure. Water molecules were added for cluster optimization in a stepwise fashion.

Structural Properties at High Temperatures. Periodic DFT-based *ab initio* molecular dynamics simulations were performed within the GGA with the exchange−correlation functional of Perdew, Burke, and Ernzerhoff (PBE)[87] and Grimme's second-generation dispersion corrections (DFT-D2)[88] as implemented in the CP2K package.[89] Detailed methods for the calculations can be found in ref 90. Starting with the optimized zeolite unit cell having Si/Al = 95,[90] AIMD simulations were performed with 1, 2, and 16 water(s) at various temperatures (27 °C ≤ T ≤ 227 °C) within the canonical *NVT* ensemble using a 0.5 fs time step and a Nose-Hoover chain thermostat to determine the local structural properties. For each simulation, well-equilibrated trajectories of ∼80 ps were collected to obtain reliable statistical properties.

■ ASSOCIATED CONTENT

Supporting Information

The Supporting Information is available free of charge on the ACS Publications website at DOI: 10.1021/jacs.8b07969.

Figures S1−S15, Table S1−S5, and optimized geometries of the structures in DFT calculation (PDF)

■ AUTHOR INFORMATION

Corresponding Authors

*Jianzhi.Hu@pnnl.gov
*Johannes.Lercher@ch.tum.de

ORCID

Meng Wang: 0000-0002-3380-3534
Nicholas R. Jaegers: 0000-0002-9930-7672
Mal-Soon Lee: 0000-0001-6851-177X
Chuan Wan: 0000-0002-8226-7619
Jian Zhi Hu: 0000-0001-8879-747X
Donghai Mei: 0000-0002-0286-4182
Donald M. Camaioni: 0000-0002-2213-0960
Oliver Y. Gutiérrez: 0000-0001-9163-4786
Vassiliki-Alexandra Glezakou: 0000-0001-6028-7021
Roger Rousseau: 0000-0003-1947-0478
Yong Wang: 0000-0002-8460-7410
Johannes A. Lercher: 0000-0002-2495-1404

Notes

The authors declare no competing financial interest.

■ ACKNOWLEDGMENTS

This work was supported by the U.S. Department of Energy, Office of Science, Office of Basic Energy Sciences, Division of Chemical Sciences, Geosciences, and Biosciences. Portions of the work were performed at the William R. Wiley Environmental Molecular Science Laboratory, a national scientific user facility sponsored by the DOE's Office of Biological and Environmental Research located at Pacific Northwest National Laboratory, a multiprogram national laboratory operated for the DOE by Battelle Memorial Institute. Additional ^{1}H MAS NMR spectra were obtained using a Bruker 600 MHz NMR spectrometer acquired with support from the U.S. Department of Energy, Office of Science, Office of Basic Energy Sciences (Project Number 66628).

■ REFERENCES

(1) Kramer, G. J.; van Santen, R. A.; Emeis, C. A.; Nowak, A. K. Understanding the acid behaviour of zeolites from theory and experiment. *Nature* **1993**, *363* (6429), 529−531.
(2) Vermeiren, W.; Gilson, J.-P. Impact of Zeolites on the Petroleum and Petrochemical Industry. *Top. Catal.* **2009**, *52* (9), 1131−1161.
(3) Martínez, C.; Corma, A. Inorganic molecular sieves: Preparation, modification and industrial application in catalytic processes. *Coord. Chem. Rev.* **2011**, *255* (13−14), 1558−1580.
(4) Primo, A.; Garcia, H. Zeolites as catalysts in oil refining. *Chem. Soc. Rev.* **2014**, *43* (22), 7548−7561.
(5) Corma, A. Inorganic Solid Acids and Their Use in Acid-Catalyzed Hydrocarbon Reactions. *Chem. Rev.* **1995**, *95* (3), 559−614.
(6) Jentoft, F. C.; Gates, B. C. Solid-acid-catalyzed alkane cracking mechanisms: evidence from reactions of small probe molecules. *Top. Catal.* **1997**, *4* (1), 1−13.
(7) de Klerk, A.; Nel, R. J. J. Phenol Alkylation with 1-Octene on Solid Acid Catalysts. *Ind. Eng. Chem. Res.* **2007**, *46* (22), 7066−7072.
(8) Zhang, M.; Yu, Y. Dehydration of Ethanol to Ethylene. *Ind. Eng. Chem. Res.* **2013**, *52* (28), 9505−9514.
(9) Okuhara, T. Water-Tolerant Solid Acid Catalysts. *Chem. Rev.* **2002**, *102* (10), 3641−3666.
(10) Liu, Y.; Vjunov, A.; Shi, H.; Eckstein, S.; Camaioni, D. M.; Mei, D.; Baráth, E.; Lercher, J. A. Enhancing the catalytic activity of hydronium ions through constrained environments. *Nat. Commun.* **2017**, *8*, 14113.
(11) Haw, J. F.; Xu, T.; Nicholas, J. B.; Goguen, P. W. Solvent-assisted proton transfer in catalysis by zeolite solid acids. *Nature* **1997**, *389* (6653), 832−835.
(12) Dai, W.; Wang, C.; Yi, X.; Zheng, A.; Li, L.; Wu, G.; Guan, N.; Xie, Z.; Dyballa, M.; Hunger, M. Identification of tert-Butyl Cations in Zeolite H-ZSM-5: Evidence from NMR Spectroscopy and DFT Calculations. *Angew. Chem., Int. Ed.* **2015**, *54* (30), 8783−6.
(13) Simperler, A.; Bell, R. G.; Anderson, M. W. Probing the Acid Strength of Brønsted Acidic Zeolites with Acetonitrile: Quantum Chemical Calculation of 1H, 15N, and 13C NMR Shift Parameters. *J. Phys. Chem. B* **2004**, *108* (22), 7142−7151.
(14) Wang, Q.; Fan, H.; Wu, S.; Zhang, Z.; Zhang, P.; Han, B. Water as an additive to enhance the ring opening of naphthalene. *Green Chem.* **2012**, *14* (4), 1152−1158.
(15) Chen, K. Z.; Damron, J.; Pearson, C.; Resasco, D.; Zhang, L.; White, J. L. Zeolite Catalysis: Water Can Dramatically Increase or Suppress Alkane C-H Bond Activation. *ACS Catal.* **2014**, *4* (9), 3039−3044.
(16) Shi, D.; Faria, J.; Pham, T. N.; Resasco, D. E. Enhanced Activity and Selectivity of Fischer−Tropsch Synthesis Catalysts in Water/Oil Emulsions. *ACS Catal.* **2014**, *4* (6), 1944−1952.
(17) Chen, K. Z.; Kelsey, J.; White, J. L.; Zhang, L.; Resasco, D. Water Interactions in Zeolite Catalysts and Their Hydrophobically Modified Analogues. *ACS Catal.* **2015**, *5* (12), 7480−7487.
(18) Zhi, Y.; Shi, H.; Mu, L.; Liu, Y.; Mei, D.; Camaioni, D. M.; Lercher, J. A. Dehydration Pathways of 1-Propanol on HZSM-5 in the Presence and Absence of Water. *J. Am. Chem. Soc.* **2015**, *137* (50), 15781−15794.
(19) Liu, Y.; Baráth, E.; Shi, H.; Hu, J.; Camaioni, D. M.; Lercher, J. A. Solvent-determined mechanistic pathways in zeolite-H-BEA-catalysed phenol alkylation. *Nature Catalysis* **2018**, *1* (2), 141−147.
(20) Eckstein, S.; Hintermeier, P. H.; Olarte, M. V.; Liu, Y.; Baráth, E.; Lercher, J. A. Elementary steps and reaction pathways in the aqueous phase alkylation of phenol with ethanol. *J. Catal.* **2017**, *352*, 329−336.
(21) Kyte, J.; Doolittle, R. F. A simple method for displaying the hydropathic character of a protein. *J. Mol. Biol.* **1982**, *157* (1), 105−132.

DOI: 10.1021/jacs.8b07969
J. Am. Chem. Soc. 2019, 141, 3444−3455

(22) van Bokhoven, J. A.; Koningsberger, D. C.; Kunkeler, P.; van Bekkum, H. Influence of Steam Activation on Pore Structure and Acidity of Zeolite Beta: An Al K Edge XANES Study of Aluminum Coordination. *J. Catal.* **2002**, *211* (2), 540−547.
(23) Bugaev, L. A.; van Bokhoven, J. A.; Sokolenko, A. P.; Latokha, Y. V.; Avakyan, L. A. Local Structure of Aluminum in Zeolite Mordenite as Affected by Temperature. *J. Phys. Chem. B* **2005**, *109* (21), 10771−10778.
(24) Drake, I. J.; Zhang, Y.; Gilles, M. K.; Teris Liu, C. N.; Nachimuthu, P.; Perera, R. C. C.; Wakita, H.; Bell, A. T. An In Situ Al K-Edge XAS Investigation of the Local Environment of H+- and Cu +-Exchanged USY and ZSM-5 Zeolites. *J. Phys. Chem. B* **2006**, *110* (24), 11665−11676.
(25) Jentys, A.; Warecka, G.; Derewinski, M.; Lercher, J. A. Adsorption of water on ZSM 5 zeolites. *J. Phys. Chem.* **1989**, *93* (12), 4837−4843.
(26) Zecchina, A.; Geobaldo, F.; Spoto, G.; Bordiga, S.; Ricchiardi, G.; Buzzoni, R.; Petrini, G. FTIR Investigation of the Formation of Neutral and Ionic Hydrogen-Bonded Complexes by Interaction of H-ZSM-5 and H-Mordenite with CH3CN and H2O: Comparison with the H-NAFION Superacidic System. *J. Phys. Chem.* **1996**, *100* (41), 16584−16599.
(27) Mihaleva, V. V.; van Santen, R. A.; Jansen, A. P. J. Quantum chemical calculation of infrared spectra of acidic groups in chabazite in the presence of water. *J. Chem. Phys.* **2004**, *120* (19), 9212−9221.
(28) Cailliez, F.; Stirnemann, G.; Boutin, A.; Demachy, I.; Fuchs, A. H. Does Water Condense in Hydrophobic Cavities? A Molecular Simulation Study of Hydration in Heterogeneous Nanopores. *J. Phys. Chem. C* **2008**, *112* (28), 10435−10445.
(29) Luz, Z.; Vega, A. J. Interaction of H-rho zeolite with water and methanol studied by multinuclear NMR spectroscopy. *J. Phys. Chem.* **1987**, *91* (2), 374−382.
(30) Vega, A. J.; Luz, Z. Characterization of NH4-rho and vacuum-calcined H-rho zeolites by multinuclear NMR spectroscopy. *J. Phys. Chem.* **1987**, *91* (2), 365−373.
(31) Sauer, J. Acidic sites in heterogeneous catalysis: structure, properties and activity. *J. Mol. Catal.* **1989**, *54* (3), 312−323.
(32) Batamack, P.; Doremieux-Morin, C.; Fraissard, J.; Freude, D. Broad-line and high-resolution NMR studies concerning the hydroxonium ion in HZSM-5 zeolites. *J. Phys. Chem.* **1991**, *95* (9), 3790−3796.
(33) Hunger, M.; Freude, D.; Pfeifer, H. Magic-angle spinning nuclear magnetic resonance studies of water molecules adsorbed on Bronsted- and Lewis-acid sites in zeolites and amorphous silica-aluminas. *J. Chem. Soc., Faraday Trans.* **1991**, *87* (4), 657−662.
(34) Batamack, P.; Doremieux-Morin, C.; Vincent, R.; Fraissard, J. Broad-line proton NMR: a new application for studying the Broensted acid strength of solids. *J. Phys. Chem.* **1993**, *97* (38), 9779−9783.
(35) Heeribout, L.; Batamack, P.; Dorémieux-Morin, C.; Vincent, R.; Fraissard, J. Proceedings of International Symposium on Magnetic Resonance in Colloid and Interface ScienceStudy of H-ZSM-5 acidity by 1H NMR: broad-line at 4 K and high resolution MAS at 300 K; Brønsted acidity scale and comparison with other zeolites. *Colloids Surf., A* **1996**, *115*, 229−237.
(36) Hunger, M.; Horvath, T. Adsorption of Methanol on Brønsted Acid Sites in Zeolite H-ZSM-5 Investigated by Multinuclear Solid-State NMR Spectroscopy. *J. Am. Chem. Soc.* **1996**, *118* (49), 12302−12308.
(37) Heeribout, L.; Dorémieux-Morin, C.; Nogier, J. P.; Vincent, R.; Fraissard, J. Study of high-silica H-ZSM-5 acidity by 1H NMR techniques using water as base. *Microporous Mesoporous Mater.* **1998**, *24* (1−3), 101−112.
(38) Kanellopoulos, J.; Unger, A.; Schwieger, W.; Freude, D. Catalytic and multinuclear MAS NMR studies of a thermally treated zeolite ZSM-5. *J. Catal.* **2006**, *237* (2), 416−425.
(39) Song, W.; Liu, Y.; Baráth, E.; Zhao, C.; Lercher, J. A. Synergistic effects of Ni and acid sites for hydrogenation and C−O bond cleavage of substituted phenols. *Green Chem.* **2015**, *17* (2), 1204−1218.
(40) Zheng, A.; Li, S.; Liu, S.-B.; Deng, F. Acidic Properties and Structure−Activity Correlations of Solid Acid Catalysts Revealed by Solid-State NMR Spectroscopy. *Acc. Chem. Res.* **2016**, *49* (4), 655−663.
(41) Jiao, J.; Altwasser, S.; Wang, W.; Weitkamp, J.; Hunger, M. State of Aluminum in Dealuminated, Nonhydrated Zeolites Y Investigated by Multinuclear Solid-State NMR Spectroscopy. *J. Phys. Chem. B* **2004**, *108* (38), 14305−14310.
(42) Semmer-Herlédan, V.; Heeribout, L.; Batamack, P.; Dorémieux-Morin, C.; Fraissard, J.; Gola, A.; Benazzi, E. Comparison of the acid strength of dealuminated H-faujasites determined by 1H NMR after water adsorption. *Microporous Mesoporous Mater.* **2000**, *34* (2), 157−169.
(43) Chen, K. Z.; Abdolrhamani, M.; Sheets, E.; Freeman, J.; Ward, G.; White, J. L. Direct Detection of Multiple Acidic Proton Sites in Zeolite HZSM-5. *J. Am. Chem. Soc.* **2017**, *139* (51), 18698−18704.
(44) Vjunov, A.; Wang, M.; Govind, N.; Huthwelker, T.; Shi, H.; Mei, D. H.; Fulton, J. L.; Lercher, J. A. Tracking the Chemical Transformations at the Bronsted Acid Site upon Water-Induced Deprotonation in a Zeolite Pore. *Chem. Mater.* **2017**, *29* (21), 9030−9042.
(45) Beck, L. W.; White, J. L.; Haw, J. F. 1H{27Al} Double-Resonance Experiments in Solids: An Unexpected Observation in the 1H MAS Spectrum of Zeolite HZSM-5. *J. Am. Chem. Soc.* **1994**, *116* (21), 9657−9661.
(46) Hunger, M. Bronsted acid sites in zeolites characterized by multinuclear solid-state NMR spectroscopy. *Catal. Rev.: Sci. Eng.* **1997**, *39* (4), 345−393.
(47) Huo, H.; Peng, L.; Grey, C. P. Low Temperature 1H MAS NMR Spectroscopy Studies of Proton Motion in Zeolite HZSM-5. *J. Phys. Chem. C* **2009**, *113* (19), 8211−8219.
(48) Hu, J. Z.; Wan, C.; Vjunov, A.; Wang, M.; Zhao, Z.; Hu, M. Y.; Camaioni, D. M.; Lercher, J. A. 27Al MAS NMR Studies of HBEA Zeolite at Low to High Magnetic Fields. *J. Phys. Chem. C* **2017**, *121* (23), 12849−12854.
(49) Prodinger, S.; Shi, H.; Eckstein, S.; Hu, J. Z.; Olarte, M. V.; Camaioni, D. M.; Derewinski, M. A.; Lercher, J. A. Stability of Zeolites in Aqueous Phase Reactions. *Chem. Mater.* **2017**, *29* (17), 7255−7262.
(50) Fyfe, C. A.; Feng, Y.; Grondey, H.; Kokotailo, G. T.; Gies, H. One- and two-dimensional high-resolution solid-state NMR studies of zeolite lattice structures. *Chem. Rev.* **1991**, *91* (7), 1525−1543.
(51) Multinuclear Solid-State NMR of Inorganic Materials. In *Pergamon Materials Series*; Kenneth, J. D. M.; Mark, E. S., Eds.; Pergamon, 2002; Vol. *6*.
(52) Zhou, Y.; Jin, Y.; Wang, M.; Zhang, W.; Xie, J.; Gu, J.; Wen, H.; Wang, J.; Peng, L. One-Pot Synthesis of Zeolitic Strong Solid Bases: A Family of Alkaline-Earth Metal-Containing Silicalite-1. *Chem. - Eur. J.* **2015**, *21* (43), 15412−15420.
(53) Dec, S. F.; Bronnimann, C. E.; Wind, R. A.; Maciel, G. E. Comparison of the 1H NMR analysis of solids by the CRAMPS and MAS-only techniques. *J. Magn. Reson. (1969-1992)* **1989**, *82* (3), 454−466.
(54) Pfeifer, H.; Freude, D.; Hunger, M. Nuclear magnetic resonance studies on the acidity of zeolites and related catalysts. *Zeolites* **1985**, *5* (5), 274−286.
(55) Price, W. S. Spin Dynamics: Basics of Nuclear Magnetic Resonance, 2nd edition. *Concepts Magn. Reson., Part A* **2009**, *34A* (1), 60−61.
(56) Humplik, T.; Raj, R.; Maroo, S. C.; Laoui, T.; Wang, E. N. Framework water capacity and infiltration pressure of MFI zeolites. *Microporous Mesoporous Mater.* **2014**, *190*, 84−91.
(57) Humplik, T.; Raj, R.; Maroo, S. C.; Laoui, T.; Wang, E. N. Effect of Hydrophilic Defects on Water Transport in MFI Zeolites. *Langmuir* **2014**, *30* (22), 6446−6453.
(58) Olson, D. H.; Haag, W. O.; Borghard, W. S. Use of water as a probe of zeolitic properties: interaction of water with HZSM-5. *Microporous Mesoporous Mater.* **2000**, *35−36*, 435−446.

DOI: 10.1021/jacs.8b07969
J. Am. Chem. Soc. 2019, 141, 3444−3455

(59) Trzpit, M.; Soulard, M.; Patarin, J.; Desbiens, N.; Cailliez, F.; Boutin, A.; Demachy, I.; Fuchs, A. H. The Effect of Local Defects on Water Adsorption in Silicalite-1 Zeolite: A Joint Experimental and Molecular Simulation Study. *Langmuir* **2007**, *23* (20), 10131−10139.
(60) Chen, H.; Wang, Y. Preparation of MCM-41 with high thermal stability and complementary textural porosity. *Ceram. Int.* **2002**, *28* (5), 541−547.
(61) Seredych, M.; Lison, J.; Jans, U.; Bandosz, T. J. Textural and chemical factors affecting adsorption capacity of activated carbon in highly efficient desulfurization of diesel fuel. *Carbon* **2009**, *47* (10), 2491−2500.
(62) Arı, M. U.; Ahunbay, M. G.; Yurtsever, M.; Erdem-Şenatalar, A. Molecular Dynamics Simulation of Water Diffusion in MFI-Type Zeolites. *J. Phys. Chem. B* **2009**, *113* (23), 8073−8079.
(63) Sarv, P.; Tuherm, T.; Lippmaa, E.; Keskinen, K.; Root, A. Mobility of the Acidic Proton in Broensted Sites of H-Y, H-Mordenite, and H-ZSM-5 Zeolites, Studied by High-Temperature 1H MAS NMR. *J. Phys. Chem.* **1995**, *99* (38), 13763−13768.
(64) Eckstein, S.; Hintermeier, P. H.; Zhao, R.; Baráth, E.; Shi, H.; Liu, Y.; Lercher, J. A. Influence of hydronium ions in zeolites on sorption. *Angew. Chem., Int. Ed.* **2019** DOI: 10.1002/anie.201812184.
(65) Marx, D.; Tuckerman, M. E.; Hutter, J.; Parrinello, M. The nature of the hydrated excess proton in water. *Nature* **1999**, *397*, 601.
(66) Tuckerman, M.; Laasonen, K.; Sprik, M.; Parrinello, M. Ab initio molecular dynamics simulation of the solvation and transport of hydronium and hydroxyl ions in water. *J. Chem. Phys.* **1995**, *103* (1), 150−161.
(67) Zundel, G. Study of hydration and hydrate structure as functions of the proton-acceptor properties of anions by infrared spectroscopy. *J. Struct. Chem.* **1966**, *6* (3), 363−365.
(68) Marx, D.; Chandra, A.; Tuckerman, M. E. Aqueous Basic Solutions: Hydroxide Solvation, Structural Diffusion, and Comparison to the Hydrated Proton. *Chem. Rev.* **2010**, *110* (4), 2174−2216.
(69) Agmon, N. The Grotthuss mechanism. *Chem. Phys. Lett.* **1995**, *244* (5), 456−462.
(70) Emeis, C. A. Determination of Integrated Molar Extinction Coefficients for Infrared Absorption Bands of Pyridine Adsorbed on Solid Acid Catalysts. *J. Catal.* **1993**, *141* (2), 347−354.
(71) Hu, J. Z.; Hu, M. Y.; Zhao, Z. C.; Xu, S. C.; Vjunov, A.; Shi, H.; Camaioni, D. M.; Peden, C. H. F.; Lercher, J. A. Sealed rotors for in situ high temperature high pressure MAS NMR. *Chem. Commun.* **2015**, *51* (70), 13458−13461.
(72) Jaegers, N. R.; Hu, M. Y.; Hoyt, D. W.; Wang, Y.; Hu, J. Z., Development and Application of In Situ High-Temperature, High-Pressure Magic Angle Spinning NMR. In *Modern Magnetic Resonance*; Webb, G. A., Ed.; Springer International Publishing: Cham, 2017; pp 1−19.
(73) Vega, A. J. Heteronuclear chemical-shift correlations of silanol groups studied by two-dimensional cross-polarization magic angle spinning NMR. *J. Am. Chem. Soc.* **1988**, *110* (4), 1049−1054.
(74) Kolodziejski, W.; Klinowski, J. Kinetics of Cross-Polarization in Solid-State NMR: A Guide for Chemists. *Chem. Rev.* **2002**, *102* (3), 613−628.
(75) Baba, T.; Komatsu, N.; Ono, Y.; Sugisawa, H. Mobility of the Acidic Protons in H−ZSM-5 As Studied by Variable Temperature 1H MAS NMR. *J. Phys. Chem. B* **1998**, *102* (5), 804−808.
(76) Baba, T.; Komatsu, N.; Ono, Y.; Sugisawa, H.; Takahashi, T. Nature of the acidic protons in H-mordenite and H-MCM-22 as studied by variable temperature 1H MAS NMR1. *Microporous Mesoporous Mater.* **1998**, *22* (1−3), 203−210.
(77) Fenzke, D.; Hunger, M.; Pfeifer, H. Determination of nuclear distances and chemical-shift anisotropy from 1H MAS NMR sideband patterns of surface OH groups. *J. Magn. Reson. (1969-1992)* **1991**, *95* (3), 477−483.
(78) Hunger, M.; Anderson, M. W.; Ojo, A.; Pfeifer, H. Study of the geometry and location of the bridging OH groups in aluminosilicate and silicoaluminophosphate type zeolites using 1H MAS NMR sideband analysis and CP/MAS NMR. *Microporous Mater.* **1993**, *1* (1), 17−32.
(79) Klinowski, J. Solid-state NMR studies of molecular sieve catalysts. *Chem. Rev.* **1991**, *91* (7), 1459−1479.
(80) Hunger, M. Multinuclear solid-state NMR studies of acidic and non-acidic hydroxyl protons in zeolites. *Solid State Nucl. Magn. Reson.* **1996**, *6* (1), 1−29.
(81) Munakata, H.; Koyama, T.-r.; Yashima, T.; Asakawa, N.; O-Nuki, T.; Motokura, K.; Miyaji, A.; Baba, T. Temperature Effect on 1H Chemical Shift of Hydroxyl Groups in Zeolites and Their Catalytic Activities as Solid Acids. *J. Phys. Chem. C* **2012**, *116* (27), 14551−14560.
(82) te Velde, G.; Bickelhaupt, F. M.; Baerends, E. J.; Fonseca Guerra, C.; van Gisbergen, S. J. A.; Snijders, J. G.; Ziegler, T. Chemistry with ADF. *J. Comput. Chem.* **2001**, *22* (9), 931−967.
(83) Grimme, S.; Antony, J.; Schwabe, T.; Muck-Lichtenfeld, C. Density functional theory with dispersion corrections for supramolecular structures, aggregates, and complexes of (bio)organic molecules. *Org. Biomol. Chem.* **2007**, *5* (5), 741−758.
(84) Van Lenthe, E.; Baerends, E. J. Optimized Slater-type basis sets for the elements 1−118. *J. Comput. Chem.* **2003**, *24* (9), 1142−1156.
(85) Mei, D. H.; Lercher, J. A. Mechanistic insights into aqueous phase propanol dehydration in H-ZSM-5 zeolite. *AIChE J.* **2017**, *63* (1), 172−184.
(86) Jones, A. J.; Carr, R. T.; Zones, S. I.; Iglesia, E. Acid strength and solvation in catalysis by MFI zeolites and effects of the identity, concentration and location of framework heteroatoms. *J. Catal.* **2014**, *312*, 58−68.
(87) Perdew, J. P.; Burke, K.; Ernzerhof, M. Generalized gradient approximation made simple. *Phys. Rev. Lett.* **1996**, *77* (18), 3865−3868.
(88) Grimme, S. Semiempirical GGA-type density functional constructed with a long-range dispersion correction. *J. Comput. Chem.* **2006**, *27* (15), 1787−1799.
(89) VandeVondele, J.; Krack, M.; Mohamed, F.; Parrinello, M.; Chassaing, T.; Hutter, J. QUICKSTEP: Fast and accurate density functional calculations using a mixed Gaussian and plane waves approach. *Comput. Phys. Commun.* **2005**, *167* (2), 103−128.
(90) Alexopoulos, K.; Lee, M.-S.; Liu, Y.; Zhi, Y.; Liu, Y.; Reyniers, M.-F.; Marin, G. B.; Glezakou, V.-A.; Rousseau, R.; Lercher, J. A. Anharmonicity and Confinement in Zeolites: Structure, Spectroscopy, and Adsorption Free Energy of Ethanol in H-ZSM-5. *J. Phys. Chem. C* **2016**, *120* (13), 7172−7182.

DOI: 10.1021/jacs.8b07969
J. Am. Chem. Soc. 2019, 141, 3444−3455